

Integration of Hyperspectral Imagery and Sparse Sonar Data for Shallow Water Bathymetry Mapping

Liang Cheng, Lei Ma, Wenting Cai, Lihua Tong, Manchun Li, and Peijun Du

Abstract—Accurate and rapid mapping of shallow water bathymetry is essential for the safe operation of many industries. Here, we propose a new approach to shallow water bathymetry mapping that integrates hyperspectral image and sparse sonar data. Our approach includes two main steps: dimensional reduction of Hyperion images and interpolation of sparse sonar data. First, we propose a new algorithm, i.e., a sonar-based semisupervised Laplacian eigenmap (LE) using both spatial and spectral distance, for dimensional reduction of Hyperion imagery. Second, we develop a new algorithm to interpolate sparse sonar points using a 3-D information diffusion method with homogeneous regions. These homogeneous regions are derived from the segmentation of the dimensional reduction results based on depth. We conduct the experimental comparison to confirm the applicability of the dimensional reduction and interpolation methods and their advantages over previously described methods. The proposed dimensional reduction method achieves better dimensional results than unsupervised method and semisupervised LE method (using only spectral distance). Furthermore, the bathymetry retrieved using the proposed method is more precise than that retrieved using common interpolation methods.

Index Terms—Bathymetry mapping, data integration, hyperspectral image, sparse sonar data.

Manuscript received March 18, 2014; revised July 11, 2014, October 11, 2014, and October 24, 2014; accepted November 17, 2014. This work was supported in part by the National Natural Science Foundation of China under Grant 41371017 and Grant 41001238 and in part by the National Key Technology R&D Program of China under Grant 2012BAH28B02.

L. Cheng is with the Jiangsu Provincial Key Laboratory of Geographic Information Science and Technology, Nanjing University, Nanjing 210023, China; with the Collaborative Innovation Center for the South Sea Studies, Nanjing University, Nanjing 210023, China; with the Collaborative Innovation Center of Novel Software Technology and Industrialization, Nanjing University, Nanjing 210023, China; and also with the Department of Geographic Information Science, Nanjing University, Nanjing 210093, China (e-mail: lcheng@nju.edu.cn).

L. Ma and L. Tong are with the Jiangsu Provincial Key Laboratory of Geographic Information Science and Technology, Nanjing University, Nanjing 210023, China, and also with the Department of Geographic Information Science, Nanjing University, Nanjing 210093, China.

W. Cai is with the Guangdong Electric Power Design Institute, Guangdong 510600, China.

M. Li and P. Du are with the Jiangsu Provincial Key Laboratory of Geographic Information Science and Technology, Nanjing University, Nanjing 210023, China; with the Collaborative Innovation Center for the South Sea Studies, Nanjing University, Nanjing 210023, China; and also with the Department of Geographic Information Science, Nanjing University, Nanjing 210093, China (e-mail: limanchun_nju@nju.edu.cn).

Color versions of one or more of the figures in this paper are available online at <http://ieeexplore.ieee.org>.

Digital Object Identifier 10.1109/TGRS.2014.2372787

I. INTRODUCTION

SHALLOW water bathymetry mapping is essential for navigation, fishery, offshore oil exploration, pipeline laying, and many other activities [1]. In coastal areas, intensive sediment transport due to, for example, tidal movements, wave propagation, and bottom currents results in significant temporal and spatial changes to underwater topography [2]. Such intensive and frequent changes demand efficient and recursive updating of bathymetric information [3]. Consequently, practical techniques have been sought that can obtain general bathymetry for coastal areas both rapidly and economically [4]. Currently, scholars have paid more attention to LiDAR for bathymetry, since LiDAR does not require for concurrently acquired sea-truth bathymetric data. LiDAR generates accurate bathymetric information over clear waters at a depth up to 70 m [5]. However, this method is limited by its expense and a narrow swath. Hence, it is not our focus in this paper. To find a rapid and economical strategy of bathymetry, here, we still consider more traditional echo sounders and optical remote sensing technology.

Bathymetry has conventionally been mapped using shipborne echo sounders, which are able to generate accurate depth points [3]. This technology has improved with time with the introduction of more accurate and reliable equipment [6]. Currently, main echo sounder technologies include Single-Beam Echo Sounders (SBES) and MultiBeam Echo Sounders (MBES). MBES can provide continuous acoustic coverage of large swaths of the seafloor, and most of the literature has suggested that multibeam technology is largely fulfilling the potential of bathymetry [7]. However, the use of MBES has not yet become economical owing to its high equipment and computational costs. Conversely, inexpensive SBES is now relatively commonplace [8] and can reach the same level of precision as MBES [9]. Owing to its narrow observation mode, SBES provides detailed information along ship routes but cannot convey changes in the broader coastal environment [4]. Moreover, environmental conditions and technological restraints prevent echo sounders' applicability in nearshore waters because shallow coastal waters are hazardous to navigate, particularly at low tides [5]. In addition, echo sounder systems are not capable of measuring depth in very shallow water, and bathymetry coverage is usually incomplete in coastal and inland waters. Mostly, the utility of bathymetric data from each echo sounder is highly dependent on the resolution at which it is collected. Spatial interpolation is a classic solution for this

TABLE I
EVALUATION OF BATHYMETRIC METHODS

Method	Price	Accuracy	Coverage	Accessibility in shallow waters
LiDAR	Expensive	High	Small	Easy
SBES	Cheap	High	Small	Difficult
MBES	Expensive	High	Large	Difficult
Optical Remote Sensing	Cheap	Low	Large	Easy

problem. While this approach requires no data other than depth measurements, the accuracy strongly depends on the geometry of measured and interpolated points and the spatial dependence of water depth [10].

Many interpolation and geostatistics methods were developed to predict values of spatial phenomena in unsampled locations [11]. Typical examples are conditions based on geostatistical concepts (kriging) and locality [inverse distance weighted (IDW) interpolation] [12]. Many factors affect the performance of spatial interpolation methods. These include: sampling density, sample spatial distribution, sample clustering, surface type, data variance, data normality, quality of secondary information, stratification, and grid size or resolution [13]. Here, we mainly consider sampling density and spatial distribution to improve accuracy of bathymetry mapping through geostatistics, which is achieved by combining with remote sensing imagery.

The optical remote sensing technique has become a viable alternative to classical methods of bathymetry mapping [3]. Bathymetry mapping using optical remote sensing techniques is cheap over large spatial extents [14]. However, accuracy of the retrieved water depth is difficult to predict, because it is influenced by factors including atmospheric absorption and scattering, water surface conditions, in-water constituents, and substrate reflectance properties. Furthermore, *a priori* or empirical knowledge is required for the retrieval technique and is not always available.

Table I presents an evaluation of the principal bathymetric methods, including both echo sounder and remote sensing methods. MBES can acquire accurate bathymetry over large areas, although its cost is very high. Conversely, SBES offer similar accuracy but at a much lower cost than that of MBES; in these cases, the low cost is offset by the limited coverage. Thus, the generation of extensive bathymetric coverage from sparse but accurate sonar points is an issue that merits further study. It is clear that shipboard echo sounder methods and optical remote sensing methods are strongly complementary (see Table I) [15]; this suggests that shallow water bathymetry mapping could be achieved by the integration of cheap, sparse, and accurate sonar points with remotely sensed optical images that offer real-time data over large spatial and temporal extents. Similar researches, integration of laser scanning points and optical images for information extraction and 3-D reconstruction,

have been reported [16]–[18]. Accordingly, we combine these techniques here to map the bathymetry of shallow water areas. We use SBES data as the sparse sonar data source, owing to its high accuracy and cheap price. Lee and Carder demonstrated that reliable derivation of bathymetry from spectral remote sensing images requires a sensor with hyperspectral capability [19]. Hyperion has more than 200 bands covering 430–2400 nm and a spatial resolution of about 30 m; even low signal-to-noise ratio, it is well suited to divide shallow area into homogeneous depth regions for bathymetric mapping in this context [4].

Therefore, we propose a new approach for integrating Hyperion images and sparse sonar data (SBES data) that includes three main steps. 1) We conduct two preprocessing steps: Hyperion preprocessing and sonar data preprocessing. 2) We propose a new algorithm for Hyperion dimensional reduction: a sonar-based semisupervised LE using spatial and spectral distance metrics. In this algorithm, sonar points are clustered as sample points of the semisupervised LE, such that the dimensional reduction result is related to water depth. Spatial distance metrics are then used in the semisupervised LE to improve existing spectral distance metrics, initiating a tendency for adjacent pixels in high-dimensional space to cluster in low-dimensional manifold space. 3) We conduct data interpolation as follows. Based on the dimensional reduction results, a multi-scale segmentation algorithm is used for deriving homogeneous depth regions. With the homogeneous regions, a new algorithm, i.e., 3-D information diffusion algorithm, is introduced for the interpolation of sparse sonar points.

This paper is structured as follows. In Section II, we review the remote sensing retrieval of bathymetry, nonlinear manifold learning dimensional reduction, and spatial interpolation. In Section III, we describe the proposed bathymetry mapping approach in details. We introduce the test data set in Section IV-A, before we discuss the experimental results in Section IV-B and C. Finally, we draw conclusions in Section V.

II. RELATED WORK

A. Review of Remote Sensing Retrieval of Bathymetry

Remote sensing retrieval of bathymetry requires a model between radiance values on satellite imagery and water depth. This model can be theoretical, semiempirical, and statistical. Theoretical models are based on radiative transfer models of water in visible bands. With the development of measure instrument, it becomes possible to measure the internal light field of water. Hence, the optical characteristics of water attract more attention, and more high-accuracy radiative transfer models are developed [20]. Ji *et al.* proposed a modified model in turbid waters [21], whereas the modified and rescaled model by Philpot (1989) may be used in areas of homogeneous water optical properties [22]. Lee *et al.* [15] utilized the Hydrolight model [23] as the basis for generating a semianalytical hyperspectral inversion model. Lyzenga *et al.* [24] proposed a simple physical algorithm to estimate bathymetry, in which information in other multispectral bands is not used. Legleiter and Roberts [25] constructed a framework for forward models

TABLE II
COMPARISON OF THREE TYPES OF INVERSION METHOD

	Theoretical models	Semi-empirical models	Statistical models
Theoretical basis	Radiative transfer model	Radiative decay	Machine learning, Artificial intelligence
Number of parameters	Many	Some	Few
Obtaining parameters	Difficult	Easy	Easy
Retrieval Accuracy	Low	Low	High

based on radiation transmission and analyzed the accuracy and limitations of remote sensing retrieval of bathymetry.

In comparison with theoretical models, semiempirical models are much simpler and easy to use, which integrate radiative decay models with empirical parameters for bathymetry retrieval; such models can be classified into single-band models and multiband models. The single-band models were first developed in the 1960s [26], [27], and high retrieval accuracy can be obtained using this model; comparing with single-band models, multiband models make comprehensive use of more than two wavebands for bathymetry retrieval. For example, Spitzer and Dirks [28] introduced a multiband retrieval model based on a two-flow radiation model. Bierwirth *et al.* [29] introduced a bathymetry retrieval model that incorporated the effects of substances at the water bottom.

Statistical models that are based on the relationship between bathymetry and the factors that affect it incorporate various statistical methods for bathymetry retrieval. Early in the 1970s, Lyzenga [30] derived a relationship between bathymetry and radiation intensity through hypothesis verification and used the principal component analysis method for bathymetry retrieval. Cracknell and Ibrahim [31] constructed a model for bathymetry retrieval by performing a regression analysis between the visible bands of MOMS and measured bathymetry. Sandidge and Holyer [32] introduced a machine learning method into bathymetry retrieval for the first time, and the retrieval results for this method exhibited better accuracy than those of traditional methods.

According to above, implementations of the optical method are very efficient for mapping bathymetry over a large area, although the range of detectable depths is reduced [5] comparing with LiDAR. All of the methods also described possess both advantages and disadvantages, particularly in terms of theoretical basis, number of parameters required, difficult of obtaining the relevant parameters, and retrieval accuracy (see Table II). The application of both theoretical and semiempirical models is restricted by many factors, including the optical characteristics of parameters of water. Moreover, the retrieval accuracy of these methods is poor. Conversely, statistical models may exhibit higher retrieval accuracy but require many water depth measurements, which limit the spread of such models somewhat.

B. Review of Nonlinear Manifold Learning Dimensional Reduction

The manifold learning method was first introduced by Seung and Lee [33], who found that only a few variables were sufficient for description of a cell group's trigger rate, i.e., that the activity of neurons could be controlled by an intrinsic low-dimensional structure. Moreover, they concluded that perception existed in the form of a manifold. Based on manifold learning theory, nonlinear manifold dimensional reduction methods were introduced by Tenenbaum *et al.* [34] and Roweis and Saul [35], who proposed the isometric mapping (ISOMAP) and locally linear embedding (LLE) methods, respectively. Subsequently, based on the Laplacian–Beltrami operator, Belkin and Niyogi [36] transferred the minimization of objective functions to an eigendecomposition problem and designed the Laplacian eigenmap (LE) method. The LE method was linearized by He *et al.* [37], who proposed the locality preserving projection method. Zhang and Zha [38] used local tangent space in hyperspectral data for the description of local properties and proposed the local tangent space alignment algorithm. Bachmann *et al.* [39] examined the accuracy of manifold coordinate representations as a reduced representation of hyperspectral imagery lookup table for bathymetry retrieval. A review on manifold-learning-based feature extraction for classification of hyperspectral data can be seen in Lunga *et al.* [40].

With the development of manifold dimensional reduction methods, supervised and semisupervised manifold dimensional reduction methods have become the subject of many researches, because these methods produce results more suitable for classification and identification [41]. Yang *et al.* [41] applied semisupervised theory to manifold dimensional reduction, making full use of sample points and Laplacian–Beltrami operators for the construction of optimal embedding. Their results indicated that semisupervised manifold learning methods can achieve more precise results than traditional methods and that the results of dimensional reduction are more suited to classification of information.

C. Review of Geostatistics and Spatial Interpolation

Spatial interpolation techniques can be used and broadly classified into two main groups: deterministic and geostatistical [42]. The most frequently used deterministic methods in spatial interpolation are the Thiessen polygon and IDW. The geostatistical method constitutes a discipline involving mining engineering, mathematics, and earth sciences [13], which there are several possibilities to incorporate secondary data to improve primary data [42]. Further and extensive analysis about geostatistics and spatial interpolation has been employed into the geosciences, soil sciences, water resources, environmental sciences, and so on. Schuurmans *et al.* [43] used range corrected daily radar composites to integrate into two methods of geostatistics, and it proved to be more accurate than a method using rainfall alone. Velasco-Forero *et al.* [44] and Schiemann *et al.* [45] also integrated radar data into two geostatistical methods. Moreover, Kanno *et al.* combined spatial interpolation with multispectral remote sensing for shallow water bathymetry [10], and it is a successful case of combination between

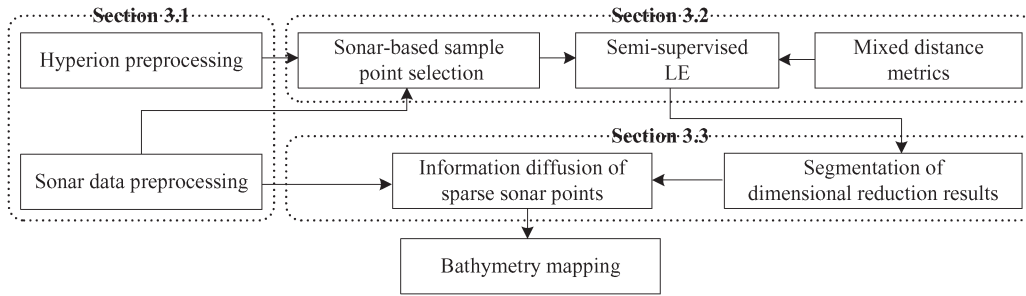


Fig. 1. Flowchart of the proposed approach.

depth-measurement data and multispectral product of QuickBird. However, QuickBird bands are limited, so that more information about water depth may be missed. Dirks *et al.* [46] compared IDW and the Thiessen polygon in interpolating rainfall data, and they recommended the use of IDW for interpolations for spatially dense networks. In general, kriging methods perform better than nongeostatistical methods [47]. Kriging and IDW are the frequently compared methods in most of the literature [13].

III. METHODOLOGY

The proposed approach includes the following three main steps (see Fig. 1): 1) data preprocessing is implemented for Hyperion data and sonar data, respectively (see Section III-A); 2) sonar-based semisupervised LE using mixed distance metrics (see Section III-B) are employed for dimensional reduction of Hyperion imagery; and 3) guided by homogeneous regions derived from segmentation of dimensional reduction results, sonar data interpolation based on 3-D information diffusion method is conducted (see Section III-C).

A. Data Preprocessing

1) *Hyperion Preprocessing*: We conduct Hyperion preprocessing in several steps: 1) scaling factor correction; 2) band subset selection; 3) bad line repair and stripe removal; 4) geometric correction; and 5) filter smoothing. During the preprocessing step, Hyperion data are scaled to limit the amount of saturation and storage space. Therefore, during 1), the digital values of the Level 1 product are 16-bit radiances and are stored as a 16-bit signed integer, and the short-wave infrared (SWIR) bands have a scaling factor of 80, and the visible and near-infrared (VNIR) bands have a scaling factor of 40 applied. Thus, we divide the radiation values in the VNIR bands by 40 and those in the SWIR bands by 80, respectively.

The Hyperion VNIR and SWIR data have 70 and 172 bands, respectively; however, a number of these bands are not illuminated, and others correspond to areas of low sensitivity of the spectrometer material. Therefore, the following bands are abandoned during 2): those not radiometrically calibrated (1–7, 58–76, 225–242), those overlapped (56–57, 77–78), and those affected by water vapor (121–127, 167–178).

Hyperion data are rotated such that the bad lines and stripes are vertical. Therefore, in 3), we adopt a bad-line-repair method proposed by Goodenough *et al.* [48] to repair bad line and a global-stripe-removal method proposed by Tan *et al.* [49] to remove the stripes. We then rotate the Hyperion data back to its original attitude.

Because the Level 1 product is only radiometrically corrected and is not geometrically resampled, here, we use Landsat imagery (the same spatial resolution with Hyperion imagery) to do geometric correction of the Hyperion imagery. Accordingly, in 4), we use a registered TM image to register the Hyperion imagery. The accuracy is controlled within half a pixel.

In general, bathymetry exhibits sharp changes. Subsequently, some stochastic noise may occur owing to bottom substances or water body and atmospheric effects. For example, in the study area used for this analysis, bathymetry exhibits sharp changes along the edge of the shipping channel. Therefore, we apply a 5×5 median filter in 5) to remove the high-frequency noise.

2) *Sonar Data Preprocessing*: There may be as many as two points per meter along the ship routes for the SBES. However, this high point density has no notable advantages for interpolation and aggravates computational complexity and memory overhead. To address this, we subsample the SBES data. The points are segmented using image pixels, and points inside the same pixel are grouped. In each group, a new point is created and endowed with the average value of the original points. The final stage of this process is to apply a correction to the ground truth to account for the tide height at the time of the Hyperion data collection.

B. Sonar-Based Semisupervised LE Using Mixed Distance Metrics

Because traditional dimensional reduction methods are based on spectral information, the dimensional results derived from such methods are lacking in spatial information. Various issues can arise, including different spectra being exhibited by the same object and different objects exhibiting the same spectrum. As pixels corresponding to deeper water in high-dimensional space tend to cluster in low-dimensional manifold space, the introduction of spatial distance metrics in dimensional reduction methods can solve the above problems effectively. Many researchers have proposed extended methods for dimensional reduction. In particular, Zhang *et al.* [50] proposed a very interesting scheme to combine the multiple features, considering the specific statistical properties of each feature. Zhang *et al.* [51] defined a tensor organization scheme for representing a pixel's spectral-spatial feature and developed tensor discriminative locality alignment for removing redundant information for subsequent classification. Mohan *et al.* [52] introduced spatial distance into the construction of a weighted undirected graph using a 3×3 window and provided an improved LLE dimensional reduction method.

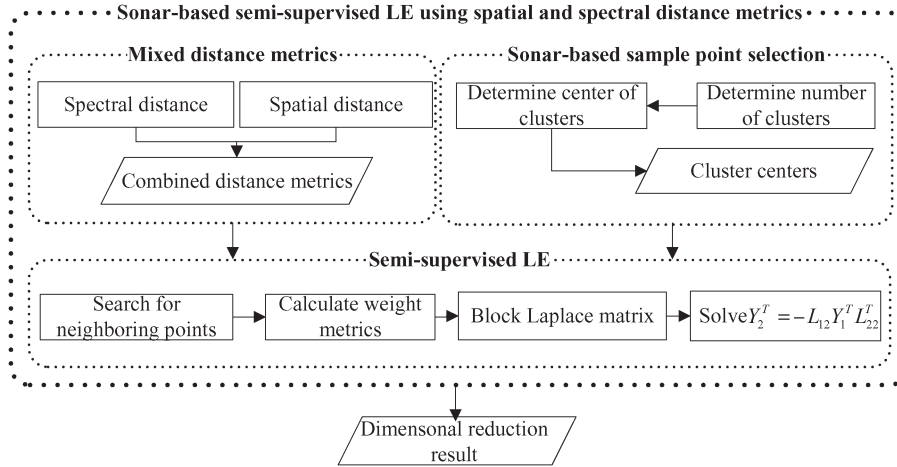


Fig. 2. Flowchart of the proposed dimensional reduction algorithm.

We propose a new dimensional reduction algorithm: a sonar-based semisupervised LE that uses spatial and spectral distance metrics (see Fig. 2). As a nonlinear manifold learning method of dimensional reduction, LE has a strong ability to resist noise and to process sparse data. However, this method does possess some disadvantages. In particular, when dealing with certain remote sensing images, the classification and identification accuracy can be low, and the dimensional reduction results may not be appropriately related to water depth [40]. This proposed algorithm can perform the dimensional reduction of hyperspectral data effectively, and the dimensional reduction results are related to water depth, which contributes to more precise bathymetry mapping. Due to only considering the water depth, this method also ignores the effect from the water properties and bottom composition, through retaining most correlated bands with water depth. However, it does not affect the results because the hyperspectral data are used as auxiliary data to improve the interpolation, while the sonar data are as the primary data source.

1) *Mixed Distance Metrics*: In this semisupervised LE algorithm, spatial and spectral distance metrics are combined, called mixed distance metrics. We use Gaussian distance for distance metrics, and the distance metrics in the LE can be written as follows:

$$\begin{aligned}
 d_{ij}^S &= 1 - \exp\left(-\frac{\|x_i^S - x_j^S\|_2^2}{2(\sigma^S)^2}\right) \\
 &= 1 - \exp\left(-\frac{\sum_{k=1}^D (x_{ik}^S - x_{jk}^S)^2}{2(\sigma^S)^2}\right) \quad \text{Spectral distance} \\
 d_{ij}^L &= 1 - \exp\left(-\frac{\|x_i^L - x_j^L\|_2^2}{2(\sigma^L)^2}\right) \\
 &= 1 - \exp\left(-\frac{\sum_{k=1}^2 (x_{ik}^L - x_{jk}^L)^2}{2(\sigma^L)^2}\right) \quad \text{Spatial distance} \\
 d_{ij} &= d_{ij}^S + d_{ij}^L \quad \text{Combined distance.} \quad (1)
 \end{aligned}$$

Here, D depicts the numbers of spectral bands. S and L are the symbols to differentiate the spectral equation and the spatial equation, which are not used in calculation. i or j shows the number of the sample points. σ^S and σ^L are the magnitude-adjusting parameters that control the difference in magnitude between spectral distance and spatial distance. The spatial location of a pixel is merely a 2-D vector, while the spectral band number is far greater than 2. Therefore, the spectral 2-norm $\|x_i^S - x_j^S\|_2^2$ is larger than the spatial 2-norm $\|x_i^L - x_j^L\|_2^2$. Thus, a proper magnitude-adjusting parameter is needed in order to make full use of the spatial characteristics.

2) *Sonar-Based Sample Point Selection*: Here, sonar-based sample point selection is used for semisupervised LE. We use sonar points (SBES points) to guide the selection of sample points of pixels. The cluster results of sonar points are first determined. Pixels corresponding to the center of these clusters are selected as sample points for the semisupervised LE. A procedure to find optimal clusters of sonar points is as follows.

Step 1: **Determining number of clusters**. K-means algorithm is iteratively used for clustering sonar points, with the increase of cluster number. The average cluster discrepancy during the iterations is calculated. Number of cluster that corresponds to the smallest discrepancy is selected as the proper number.

Step 2: **Determining center of clusters**. Based on the determined number of clusters, clustering is performed with an increasing sample size. The average cluster discrepancy is calculated. The smallest discrepancy corresponding to sample size is selected. Center of each cluster is then determined.

3) *Semisupervised LE*: The work flow of the semisupervised LE is as follows.

Step 1: **Searching for neighboring points**. We traverse data set \vec{X} ($\vec{X} \in R^D$ depicts D -dimensional vector set, and the number of vectors is n) and seek the neighboring points for each point. During this procedure, mixed distance metrics are used. Certain number of points most close to each point should be considered

to be neighboring points. After the traversal, we construct neighboring graph G.

- Step 2: **Calculating weight metrics.** We use a kernel function to determine weight W . If x_i and x_j are connected, the weight is calculated as $w_{i,j} = \exp(-\|x_i - x_j\|^2/t)$ (t is a scale parameter to adjust the weight, generally equal to 1); otherwise, it is set 0. Because the input sets \vec{X} are partitioned as $[\vec{X}_1 \vec{X}_2]$, where $\vec{X}_1 = [x_{11}, x_{12}, \dots, x_{1m}]$ is composed of m priori sample sets (m is the number of priori samples), $\vec{X}_2 = [x_{21}, x_{22}, \dots, x_{2(n-m)}]$ is the unknown dimension data set ($n - m$ is the number). Similarly, \vec{Y} are partitioned as $[\vec{Y}_1 \vec{Y}_2]$, where $\vec{Y}_1 = [y_{11}, y_{12}, \dots, y_{1m}]$ is the low-dimensional embedding corresponding to the sample sets (it means that \vec{Y}_1 is known), $\vec{Y}_2 = [y_{21}, y_{22}, \dots, y_{2(n-m)}]$ is low-dimensional embedding coordinates of \vec{X}_2 .
- Step 3: **Blocking Laplace matrix.** We block the Laplacian matrix ($L = \begin{bmatrix} L_{11} & L_{12} \\ L_{12}^T & L_{22} \end{bmatrix}$) according to the sample data set \vec{X}_1 and its corresponding low-dimensional embedding information \vec{Y}_1 , where L_{11} is $m \times m$ matrix (m is the number of priori samples).
- Step 4: **Solving formula.** The minimization problem can be written as $\min_{Y_2} [Y_1 Y_2] \begin{bmatrix} L_{11} & L_{12} \\ L_{12}^T & L_{22} \end{bmatrix} \begin{bmatrix} Y_1^T \\ Y_2^T \end{bmatrix}$. Since Y_1 is known, we solve the formula $Y_2^T = -L_{12} Y_1^T L_{22}^{-1}$ for the low-dimensional embedding result of the whole data set \vec{X} [41], thus obtaining the dimensional reduction result Y_2^T .

C. Sonar Interpolation Integrating 3-D Information Diffusion Method With Homogeneous Regions

A satisfactory dimensional reduction result, which is related to water depth, is obtained after producing a sonar-based semisupervised LE using spatial and spectral distance metrics. For the purpose of bathymetry mapping, we introduce a new interpolation algorithm for sparse sonar points.

1) **Segmentation of Dimensional Reduction Results for Homogeneous Regions:** A multiscale segmentation method is used for homogeneous regions and consists of three steps: initial segmentation, patch merge, and attribute calculation.

- Step 1: **Initial segmentation.** Initial segmentation is performed through ENVI software, to generate a region of interest. It needs a parameter to control the size of the segmented object.
- Step 2: **Patch merge.** We use the Full Lambda-Schedule algorithm [53] to merge the same objects, which are segmented into a multiobject in the initial segmentation step. It needs a threshold to decide whether the combination between both objects is done. The segmentation and merge scales are manually determined by comparing a series of different parameters.
- Step 3: **Attribute calculation.** After the segmentation, the study area is segmented into several homogeneous

regions in which the bathymetry tends to remain consistent. Subsequently, the attribute of the object with spatial, spectral, and/or texture can be calculated to describe the region.

2) **Information Diffusion of Sparse Sonar Points in Homogeneous Regions:** Interpolation is an important step in bathymetry mapping from sonar points. Many interpolation methods exist, including kriging, IDW, and spline. However, these traditional interpolation methods require an adequate number of evenly distributed points, which is impossible for sparse sonar points. Although there are as many as two points per meter along ship routes, the distance between ship routes can reach up to 500 m, which means that sonar points are quite sparse. Thus, obvious stripes can be found in interpolated results derived using traditional interpolation methods.

In this paper, we use a 3-D information diffusion method for the interpolation of sparse sonar points. Information diffusion is a basic method in fuzzy mathematics. Single-valued samples are converted into fuzzy set-valued samples, which are expressed in the form of probabilities. Subsequently, the samples are used for fuzzy diffusion and interpolation. This method can be applied well to problems with a small sample set. The detailed procedure for information diffusion can be described as follows.

- Step 1: **Calculating minimum steps of each variable.** We calculate the minimum steps of each variable in order to construct the monitoring space. The observed values are discretized based on the minimum steps. We assume that the minimum steps are $\Delta u = \Delta x$, $\Delta v = \Delta y$, and $\Delta w = \Delta z$

$$\Delta x = \min_{x_i \neq x_j} \{|x_i - x_j|, j = 1, 2, \dots, n\} \quad (2)$$

$$\Delta y = \min_{y_i \neq y_j} \{|y_i - y_j|, j = 1, 2, \dots, n\} \quad (3)$$

$$\Delta z = \min_{z_i \neq z_j} \{|z_i - z_j|, j = 1, 2, \dots, n\} \quad (4)$$

where x_i , y_i , and z_i is the coordinate of the i th sample points ($1 \leq i \leq n$); x_j , y_j , and z_j is the coordinate of the j th sample points ($1 \leq j \leq n$); according to the minimum steps, the monitoring space ($U \times V \times W$) can be easily generated, and universes of each dimension are $U = \{u_i | i = 1, 2, \dots, m\}$, $V = \{v_j | j = 1, 2, \dots, t\}$, $W = \{w_k | k = 1, 2, \dots, s\}$, respectively; here, $u_i = u_0 + i\Delta x$, $v_j = v_0 + j\Delta y$, $w_k = w_0 + k\Delta z$, and default setting is $u_0 = v_0 = w_0 = 0$.

- Step 2: **Constructing monitoring space.** As the observing values in each dimension are $b_x = \max_{1 \leq i \leq n} \{x_i\}$, $a_x = \min_{1 \leq i \leq n} \{x_i\}$, $b_y = \max_{1 \leq i \leq n} \{y_i\}$, $a_y = \min_{1 \leq i \leq n} \{y_i\}$, $b_z = \max_{1 \leq i \leq n} \{z_i\}$, and $a_z = \min_{1 \leq i \leq n} \{z_i\}$. According to the average distance model, the diffusion coefficient h

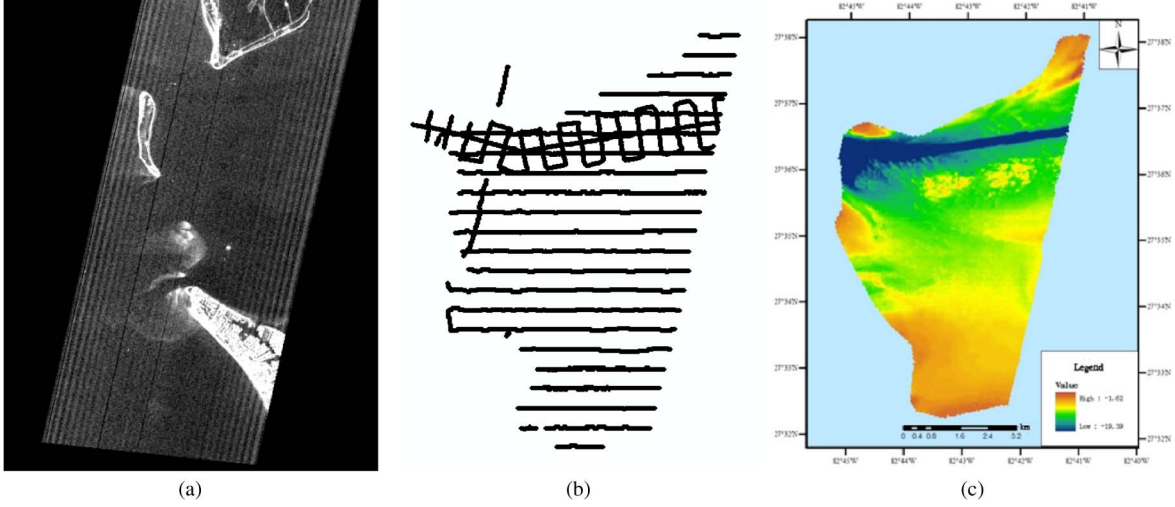


Fig. 3. Experimental data. (a) Hyperion data (Band 18). (b) SBES points. (c) Existing water bathymetry.

can be solved [54]. Thus

$$h = \begin{cases} 0.8146(b-a) & n = 5 \\ 0.5690(b-a) & n = 6 \\ 0.4560(b-a) & n = 7 \\ 0.3860(b-a) & n = 8 \\ 0.3362(b-a) & n = 9 \\ 0.2986(b-a) & n = 10 \\ 2.6851(b-a)/(n-1) & n > 10 \end{cases} \quad (5)$$

where $b = b_x$ or $b = b_y$ or $b = b_z$; $a = a_x$ or $a = a_y$ or $a = a_z$; n is the numbers of samples; h is called diffusion coefficient.

Step 3: **Calculating information diffusion of sample points.**

If we assume that the information diffusion result $Q(u, v, w)$ of sample point (x_l, y_l, z_l) in monitoring space (u_i, v_j, w_k) is $q_l(u_i, v_j, w_k)$, then its information diffusion value is defined as follows:

$$q_l(u_i, v_j, w_k) = \frac{1}{h_x \sqrt{2\pi}} \exp \left[-\frac{(u_i - x_l)^2}{2h_x^2} \right] \times \frac{1}{h_y \sqrt{2\pi}} \exp \left[-\frac{(v_j - y_l)^2}{2h_y^2} \right] \times \frac{1}{h_z \sqrt{2\pi}} \exp \left[-\frac{(w_k - z_l)^2}{2h_z^2} \right] \quad (6)$$

where h_x , h_y , and h_z are calculated by (5); l is the number of the sample point; u_i, v_j, w_k are the monitoring point, $1 \leq i \leq m, 1 \leq j \leq t, 1 \leq k \leq s$.

Step 4: **Calculating original information matrix.** We calculate the information value of each observing point in monitoring space by (6), and calculate the original information matrix Q as follows:

$$Q_{ijk} = \sum_{l=1}^n q_l(u_i, v_j, w_k) \quad (7)$$

where $q_l(u_i, v_j, w_k)$ is easily calculated by (6); l is the number of the sample point; according to

(7), original information matrix $\{Q_{ijk}\}_{m \times t \times s}$ can be generated for next work.

Step 5: **Calculating fuzzy relation matrix.** The fuzzy relation matrix is calculated using the original information matrix Q , and some method used by Wang [55]. Here, we use the R_f model [54] to change the original information matrix $\{Q_{ijk}\}_{m \times t \times s}$ into the fuzzy input-output relationship $\{r_{ijk}\}_{m \times t \times s}$

$$\begin{cases} S_k = \max_{1 \leq i \leq m, 1 \leq j \leq t} Q_{ijk}, & k = 1, 2, \dots, s \\ \mu_k(u_i, v_j) = \frac{Q_{ijk}}{S_k}, & i = 1, 2, \dots, m, \text{ and} \\ & j = 1, 2, \dots, t \\ r_{ijk} = \mu_k(u_i, v_j), & i = 1, 2, \dots, m, \\ & j = 1, 2, \dots, t, \text{ and} \\ & k = 1, 2, \dots, s. \end{cases} \quad (8)$$

Then, based on Q , we obtain a fuzzy relation $R_f = \{Q_{ijk}\}_{m \times t \times s}$, where we use the first letter “f” of factor space to indicate this kind of fuzzy relation.

Step 6: **Predicting water depth.** To predict the value of water depth, we calculate the gravity center of the fuzzy set based on the following equation:

$$R = \sum_{z \in w} \left(\frac{r_{ijk}}{w_k} \right) \quad (9)$$

where $W = \{w_k | k = 1, 2, \dots, s\}$; r_{ijk} can be calculated by (8); $1 \leq i \leq m, 1 \leq j \leq t$.

IV. EXPERIMENT

A. Datasets

We select Tampa Bay in Florida as the study area and use data including Hyperion, registered TM, sparse sonar points, and existing water bathymetry (see Fig. 3). 1) The Hyperion image used in this study is named EO1H0170412003042110PZ_AGS_01 with acquisition date in 2003/02/11. 2) We interpolate sparse sonar points for underwater topography, which is

TABLE III
DETAILS OF THE EXPERIMENTAL DATA

Data name	Acquisition Time	Source	Use
Hyperion	2003/02/11	USGS	Acquisition of homogeneous regions
Landsat TM	2003/02/19	Gulf of Mexico Integrated Science	Reference for Hyperion registration
Sparse sonar data	2001-2003	Gulf of Mexico Integrated Science	Bathymetry retrieval
Water bathymetry	2003	Gulf of Mexico Integrated Science	Validation of experimental results

collected by SBES, dating from 2001 to 2003. The average point distance along ship routes is 0.5 m, and the distance between neighboring routes is about 500 m. The total number of points is 47 550 in the research area. Its area is 48 km², and then, the density is about 990 points per square kilometer. A channel exists in this study area, where sonar points are densely measured [zigzag in Fig. 3(b)]. During the preprocessing of sonar data, sonar points are classified into two classes: normal and densely measured points. Only the normal points are subsampled. All densely measured points are retained. The subsampled points and densely measured points are then merged. 3) The TM imagery is used for the registration of Hyperion. The TM imagery used in this study is labeled LT50170412003050LGS01 with acquiring in 2003/02/19. 4) We use Tampa Bay topographic/bathymetric DEM with a resolution of 30 m to assess the accuracy of the retrieval results. It is a hybrid elevation model created from USGS topography and NOAA bathymetry data in 2003. In this paper, we focus on bathymetry, which was provided by NOAA. The best available bathymetric data were selected with a GIS query procedure that applied spatial and temporal filters to obtain 47 digital NOAA hydrographic surveys, in the Tampa Bay region. Approximately 600 000 soundings were transformed from multiple orthometric and tidal vertical datums to a common vertical reference (the NAD83 ellipsoid). Then, the bathymetry points were gridded to produce a raster surface model with a 1-arc-second (approximately 30 m) grid spacing. The details are presented in Table III.

B. Experimental Results

1) *Results of Sonar Point Clustering*: Fig. 4 illustrates the results of bathymetry mapping using our proposed approach. Table IV presents the iterative procedures for sonar points using the K-means algorithm, which generates ideal sample points for the semisupervised LE. In the first phase, the average discrepancy decreases with increasing cluster number. We select 12 as the optimal cluster number in order to avoid the presence of clusters without any sonar points. In the second phase, we consider 200 and 700 to be the best initial random point number for their corresponding smallest average discrepancies. In the third phase, we select values of around 200 and 700 as random point numbers for further clustering in order to determine the final best random point number; we consider 195 to be the optimal

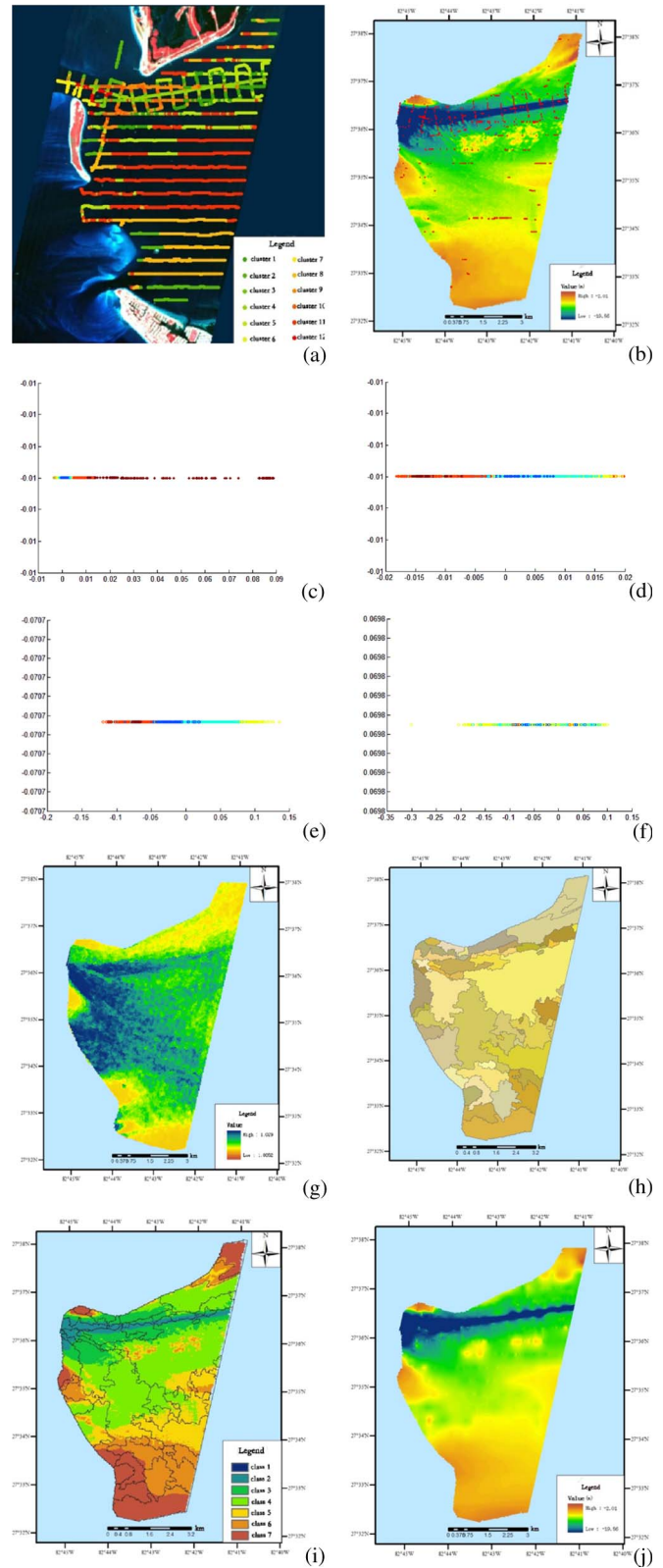


Fig. 4. Experimental procedures. (a) Clustered sonar points. (b) Sample points. (c) Distribution of pixels in two dimensions (LE). (d) Distribution of pixels in two dimensions (semisupervised LE using spectral distance metrics with clustered sample points). (e) Distribution of pixels in two dimensions (semisupervised LE using combined distance metrics with clustered sample points). (f) Distribution of pixels in two dimensions (semisupervised LE using combined distance metrics with random sample points). (g) Dimensional reduction result. (h) Result after multiscale segmentation. (i) Segmented result and clustered bathymetry. (j) Information diffusion result.

TABLE IV
CLUSTERED RESULTS OF SONAR POINTS
USING THE K-MEANS ALGORITHM

First phase									
Cluster center number	5	6	7	8	9	10	11	12	13
Average discrepancy	33.45	17.35	12.93	9.92	7.70	6.60	5.80	5.01	3.02
Second phase									
Random point number	10	100	200	300	400	500	600	700	1000
Average discrepancy	5.01	5.01	4.75	5.01	5.01	5.01	5.01	4.75	5.01
Third phase									
Random point number	190	195	205	210	690	695	705	710	715
Average discrepancy	4.75	4.74	4.88	4.75	4.75	5.01	5.01	5.01	5.01

TABLE V
CLUSTERING STATISTICS FOR SONAR POINTS

	Whole	Cluster 1	Cluster 2	Cluster 3	Cluster 4	Cluster 5	Cluster 6
Cluster center	-11.1602	-9.3621	-3.8004	-13.9071	-15.1869	-8.2899	-19.7460
Pixel number	14074	1987	523	681	2874	2145	344
	Cluster 7	Cluster 8	Cluster 9	Cluster 10	Cluster 11	Cluster 12	
Cluster center	-24.5605	-5.1402	-10.7514	-12.1251	-6.7161	-16.4174	
Pixel number	343	947	1255	827	1370	778	

random point number due to the smallest average discrepancy. Finally, we cluster sonar points with cluster number 12 and random point number 195 [see Table V; Fig. 4(a)]. Fig. 4(a) illustrates the pixels intersecting the clustered centers, i.e., the sample points for the semisupervised LE. It is clear that more pixels are selected in areas where topography has a big change, whereas fewer pixels are selected in flat areas.

2) *Results of Dimensional Reduction of Hyperion Imagery:* In order to verify the effectiveness of our proposed approach, we adopt four methods for dimensional reduction of Hyperion: unsupervised LE, semisupervised LE using spectral distance metrics with clustered sample points, semisupervised LE using spatial and spectral distance metrics with clustered sample points, and semisupervised LE using spatial and spectral distance metrics with random sample points [see Fig. 4(c)–(f), respectively]. The x -axis in Fig. 4 refers to the first band of the dimensional reduction results, the y -axis refers to the second band, and the colors of points refer to the corresponding clustered classes in the existing water bathymetry. Clustering of pixels of the same color indicates that the dimensional reduction result is easily segmented and is related to bathymetric information; such clustering indicates that the method is suitable for the generation of homogeneous bathymetry regions.

Fig. 4(c) illustrates the dimensional reduction result by using the unsupervised LE algorithm, in which clusters are unevenly distributed. Fig. 4(d) illustrates the dimensional reduction result by using the semisupervised LE using spectral distance metrics with clustered sample points, in which almost all clusters are evenly distributed. However, many mixtures remain along the boundary between clusters. The results of our proposed approach, in which the dimensional reduction results for the semisupervised LE using spatial and spectral distance metrics is used, are presented in Fig. 4(e). In this experiment, the spectral controlling parameter σ^S is set to 1 and the spatial controlling

parameter σ^L to 100. It is clear that the different clusters are separated well, and fewer mixtures are found than in the semisupervised LE using only spectral distance metrics. Because points with exiguous spectral differences may be located far away from each other, the introduction of spatial distance metrics can enhance their differences effectively, which can lead finally to the decrease of mixtures in the dimensional reduction result. In order to verify the importance of clustered sample points, we conduct the experiment in Fig. 4(f), in which a semisupervised LE using spatial and spectral distance metrics with random sample points is used. Obviously, many mixtures occur in the result, and it is difficult to separate the clusters. Therefore, the selection of sample points is quite important, reinforcing the importance of the K-means cluster method for sonar points. There is a clear difference in the pixel values on the x -axes in Fig. 4(d) and (e) (-0.02 – 0.02 and -0.15 – 0.15 , respectively). Thus, the dimensional reduction result obtained using only spectral distance metrics is shrunken compared with that obtained using both spatial and spectral distance metrics; this is inconvenient for classification and identification. Finally, the dimensional reduction result obtained by producing a semisupervised LE using spatial and spectral distance metrics with clustered sample points is presented in Fig. 4(g), and it is from this result that the overall bathymetry information is obtained.

3) *Results of Segmentation and Interpolation:* After dimensional reduction, the multiscale segmentation technique is used for the acquisition of homogeneous regions. The segmentation and merging scales are set to 62 and 91, respectively, which are manually determined by comparing a series of different parameters. The segmented homogeneous regions are illustrated in Fig. 4(h); in Fig. 4(i), these regions are overlaid on the clustered result of existing water bathymetry, and the primary structures of underwater topography can be seen clearly. Although oversegmentation and undersegmentation do occur, we find that it has little influence on the final retrieval results. These differences may be due to the fact that the hyperspectral imagery is influenced by water depth, water properties, and bottom composition. It is easy to know that bottom composition play a greater influence on segmentation results in the shallow sea, and water properties may be the influences on the results deeper in the deep sea. Essentially, the results are correlated with the water depth. Furthermore, it has little influence on the final retrieval results according to Fig. 4(i).

Finally, we use the information diffusion method for the interpolation of sonar points in each homogeneous region and obtain the shallow water bathymetry of the experimental area [see Fig. 4(j)].

C. Analysis of Comparison Experiments

Here, four strategies are used to compare the retrieved bathymetry generated by the proposed approach, IDW interpolation, and kriging interpolation, respectively. These four strategies include comparison by visual effect (see Section IV-C1), comparison by profiles (see Section IV-C2), comparison by sample points (see Section IV-C3), and comparison by global errors (see Section IV-C4).

1) *Comparison by Visual Effect:* Fig. 5 illustrates the retrieval bathymetries obtained using the proposed approach,

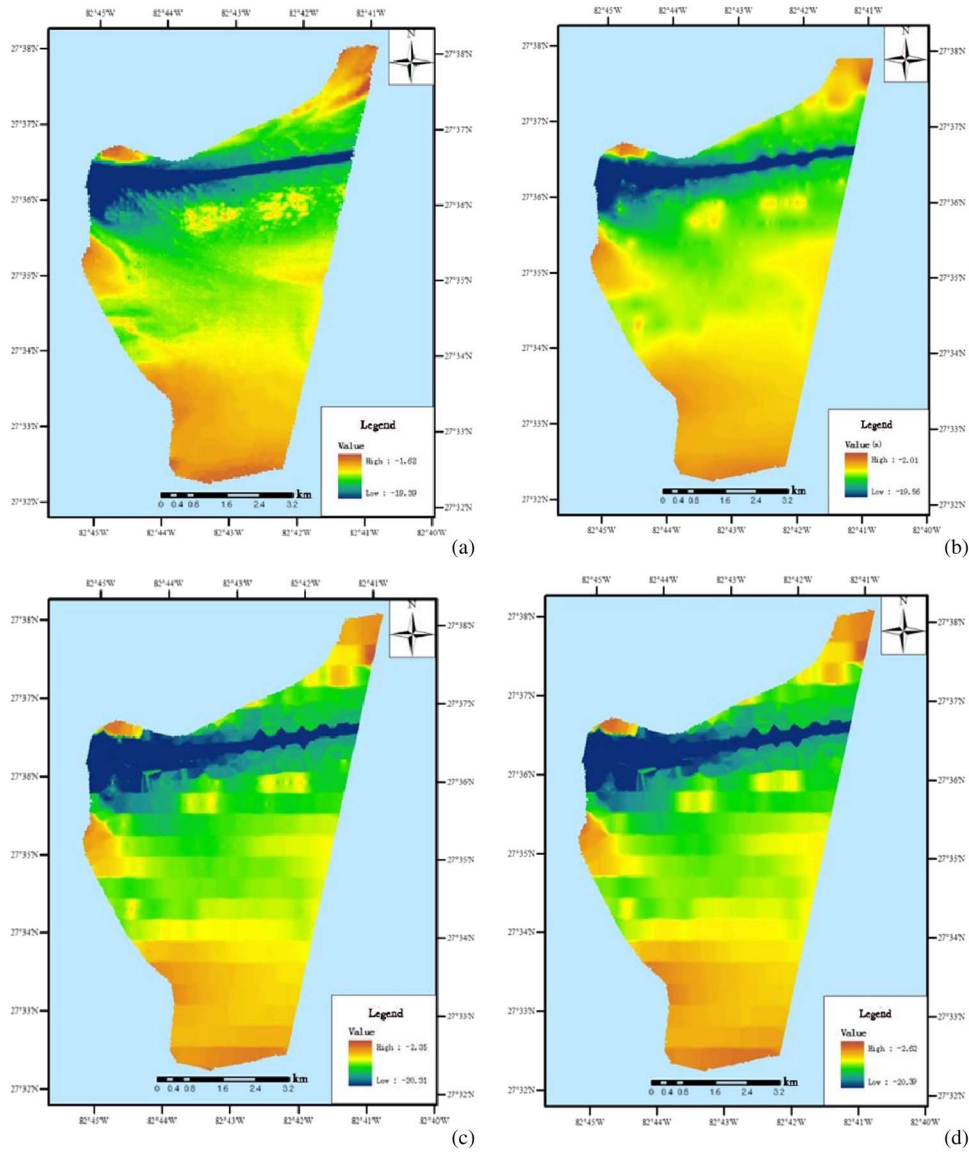


Fig. 5. Comparison of interpolated results. (a) Existing water bathymetry. (b) Result using proposed approach. (c) Result using IDW method. (d) Result using kriging method.

IDW, and kriging. It is particularly clear that there are many stripes present in Fig. 5(c) and (d) that are not present in Fig. 5(b). The bathymetry changes derived using the information diffusion method are gentle and exhibit spatial patterns that mimic those of the existing water bathymetry, except in a few small portions (e.g., terrain mutation). The channel in the northern part of the experimental area, the mapping of which is very important for activities including navigation and fishery, is well mapped. However, the IDW and kriging methods [see Fig. 5(c) and (d)] produce results in which the boundary of the channel is blocked and enlarged in comparison to the existing water bathymetry, and such confusing information could have disastrous consequences. Moreover, other underwater topographic features (e.g., basins and stages) can be seen clearly in Fig. 5(b), but are barely recognizable in Fig. 5(c) and (d).

2) *Comparison by Profiles:* In order to quantitatively compare the retrieved bathymetry, we generate three cross sections (see Fig. 6): a 6-km transect that extends along ship routes and is designed to check retrieval accuracy along the region

of dense sonar points (A); a profile oriented perpendicular to ship routes, with a length of 8 km, that is designed to verify retrieval accuracy in the region of sparse sonar points (B); and a profile that extends from the southwestern corner to the northern part of the area and traverses all primary topographic fluctuations of the study area (C). Then, for each cross section, we generate four profiles using the existing bathymetry, our proposed approach, and the IDW and kriging methods.

1) *Comparison along profile line A:* The characteristics of and relationships between the profiles generated along line A are illustrated in Fig. 7. It is clear that similar profiles are obtained for our proposed approach and the IDW and kriging methods [see Fig. 7(a)]. We obtain Pearson correlation coefficients between the existing and retrieved bathymetry for statistical analysis (see Table VI). In general, we find the coefficients to be extremely high. The coefficients between various combinations of retrieved bathymetry all exceed 0.983,

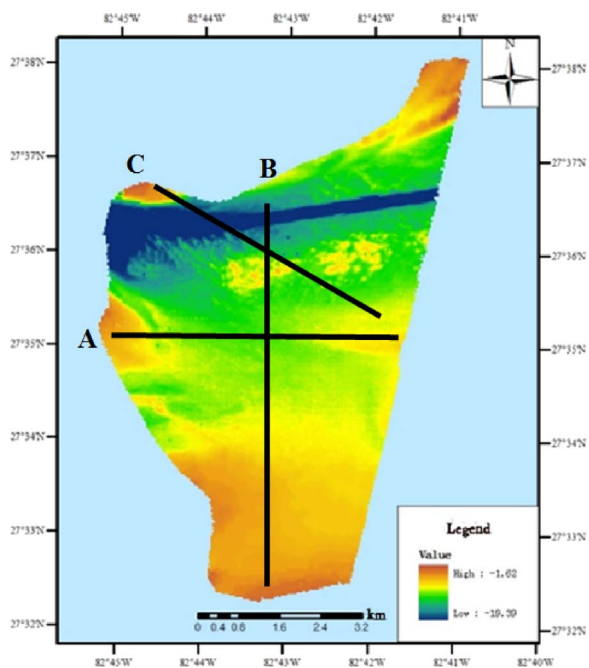


Fig. 6. Profile lines (Line A: a 6-km transect that extends along ship routes; Line B: a profile oriented perpendicular to ship routes, with a length of 8 km; Line C: a profile that extends from the southwestern corner to the northern part of the area and traverses primary topographic fluctuations of the study area).

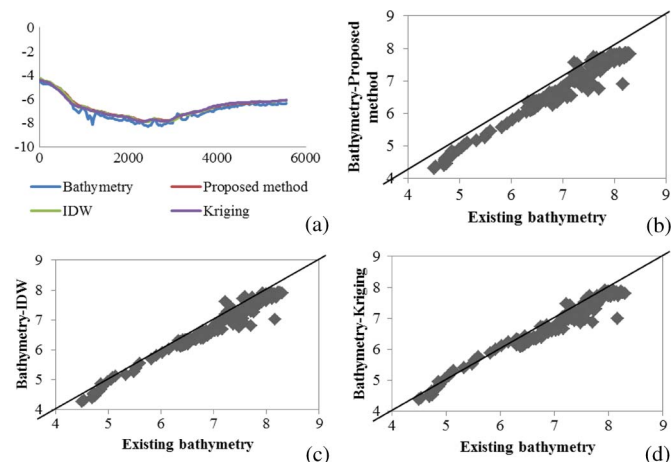


Fig. 7. Comparison of profiles along line A. (a) Cross section along line A. (b) Comparison between proposed approach and existing bathymetry. (c) Comparison between IDW and existing bathymetry. (d) Comparison between kriging and existing bathymetry.

indicating that the different methods produce almost identical bathymetry. This, perhaps, is unsurprising, because line A is located along ship routes in regions with dense sonar points.

2) *Comparison along profile line B*: Fig. 8 illustrates the characteristics of and relationships between the profiles generated along line B. Similar profiles are obtained using IDW and kriging methods (see Fig. 8(a); Table VII). However, the Pearson coefficients for the correlations between the bathymetry obtained using the IDW and kriging methods with the existing bathymetry (equal to 0.975 and 0.972, respectively) are lower than those for

TABLE VI
PEARSON CORRELATION COEFFICIENTS FOR RETRIEVED BATHYMETRY ALONG LINE A

	Bathymetry	Proposed approach	IDW	Kriging
Bathymetry	1	0.983	0.986	0.984
Proposed approach	0.983	1	0.998	0.994
IDW	0.986	0.998	1	0.997
Kriging	0.984	0.994	0.997	1

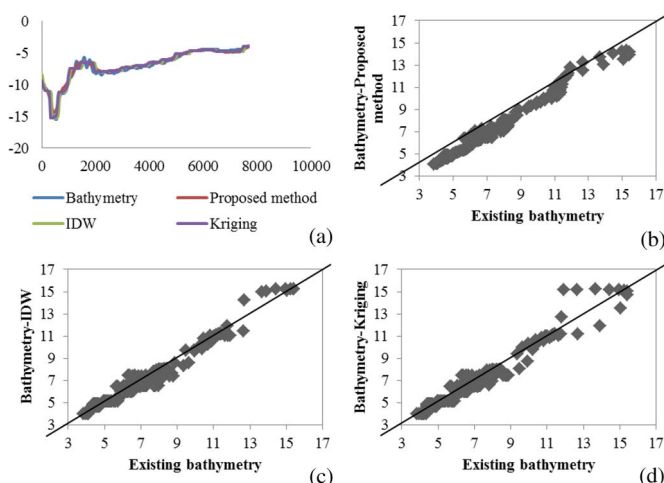


Fig. 8. Comparison of profiles along line B. (a) Cross section along line B. (b) Comparison between proposed approach and existing bathymetry. (c) Comparison between IDW and existing bathymetry. (d) Comparison between kriging and existing bathymetry.

TABLE VII
PEARSON CORRELATION COEFFICIENTS FOR RETRIEVED BATHYMETRY ALONG LINE B

	Bathymetry	Proposed approach	IDW	Kriging
Bathymetry	1	0.992	0.975	0.972
Proposed approach	0.992	1	0.985	0.987
IDW	0.975	0.998	1	0.974
Kriging	0.972	0.987	0.974	1

line A and the plots are clearly more scattered. However, the Pearson coefficient for the correlation between the bathymetry obtained using our proposed approach and the existing bathymetry is still high in this instance, and the results obtained using our proposed approach are clearly superior (see Fig. 8(b)–(d); Table VII). It is clear that all three retrieval methods produce similar, highly precise results for water depths shallower than 10 m. However, differences begin to appear when water depth exceeds 10 m. In particular, the retrieved depths for the IDW and kriging methods are considerably

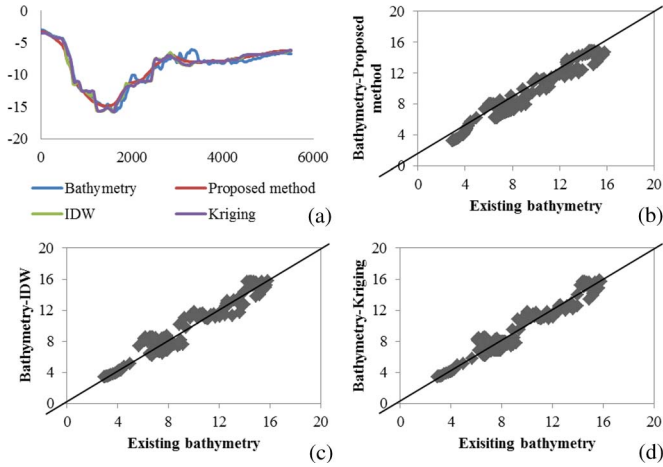


Fig. 9. Comparison of profiles along line C. (a) Cross section along line C. (b) Comparison between proposed approach and existing bathymetry. (c) Comparison between IDW and existing bathymetry. (d) Comparison between kriging and existing bathymetry.

TABLE VIII
PEARSON CORRELATION COEFFICIENTS OF RETRIEVED
BATHYMETRY ALONG LINE C

	Bathymetry	Proposed approach	IDW	Kriging
Bathymetry	1	0.975	0.966	0.971
Proposed approach	0.975	1	0.990	0.986
IDW	0.966	0.990	1	0.996
Kriging	0.971	0.986	0.996	1

different to the depths indicated by the existing bathymetry, increasing the error of the retrieved result. This phenomenon is absent in the results for our proposed approach, demonstrating that our method can retrieve bathymetry in deeper water and with more sparse sonar data than other retrieval methods.

- 3) *Comparison along profile line C*: Fig. 9 illustrates the characteristics of and relationships between the profiles generated along line C. All methods retrieve the primary topographic features, particularly the deep channel and deep cliff [see Fig. 9(a)], and the retrieved bathymetry correlates well with the existing bathymetry, with similar distributions and correlation coefficients for all methods (see Figs. 8(d)–9(b); Table VIII). However, despite this consistency, the products of our proposed approach exhibit stronger correlation with the existing bathymetry than those of IDW or kriging, although some features (particularly small local topographic features) are poorly resolved even with our method.

3) *Comparison by Sample Points*: We select 500 random sample points to compare our proposed approach with IDW and kriging methods (see Fig. 10). In Fig. 10, the figures on the left compare the existing bathymetry with that generated by various retrieval methods, whereas those on the right illustrate the errors associated with the corresponding methods. For our proposed

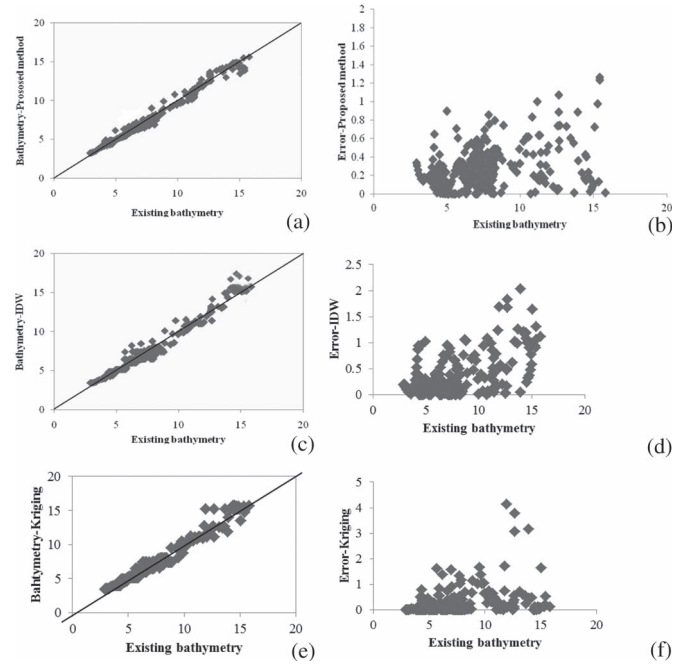


Fig. 10. Comparison by sample points. (a) Comparison between proposed approach and existing bathymetry. (b) Distribution of errors from proposed approach. (c) Comparison between IDW and existing bathymetry. (d) Distribution of errors from IDW. (e) Comparison between kriging and existing bathymetry. (f) Distribution of errors from kriging.

approach [see Fig. 10(a)], there is little scatter in the data, and the error values are centered around 0.3 m. Additionally, there is no reduction in the retrieved accuracy with increasing water depth. Nevertheless, the results of the IDW and kriging methods are considerably different. There is little spread in results for water depths below 10 m [see Figs. 9(e) and 10(c)], indicating an ideal retrieval result. However, scatter increases for water depths exceeding 10 m, indicating larger retrieval error. This is confirmed by Figs. 9(f) and 10(d), in which error increases with increasing depth of the existing bathymetry. Moreover, the errors for the IDW and kriging methods are centered around 0.5 m, i.e., larger than those of our proposed approach. Therefore, we confirm that our proposed approach can obtain more precise results that exhibit good stability across a range of water depths.

4) *Comparison by Global Errors*: We assess the global errors in retrieved bathymetry for our proposed approach and the IDW and kriging methods (see Fig. 11). We find that the error related to our proposed approach exhibits gradual changes, whereas that related to other retrieval methods exhibits abrupt changes. In order to quantitatively assess these results, we calculate the maximum, mean, and RMSE of errors for all three retrieval methods (see Table IX). Our results indicate that the maximum and mean errors are smaller for our proposed approach than that for either IDW or kriging, providing further evidence of the efficacy of our method. RMSE of our method is smaller than that of IDW and kriging. This indicates that the error value is closer to the mean value, i.e., that the results of our method are more stable than those generated by IDW and kriging.

Because large-scale topographic features can influence the retrieval results considerably, we select channel and basin areas

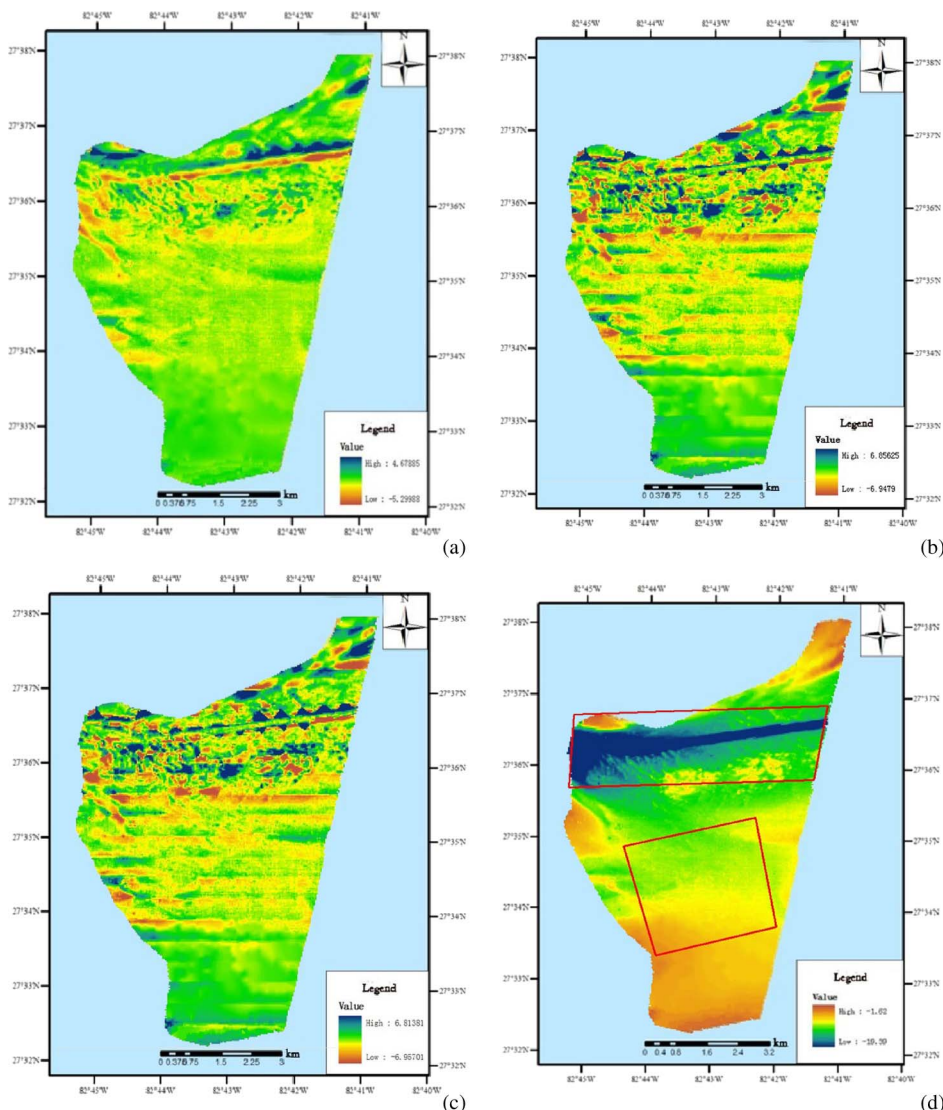


Fig. 11. Comparison by global error analysis. (a) Global error for proposed approach. (b) Global error for IDW. (c) Global error for kriging. (d) Two comparison regions.

TABLE IX
GLOBAL ERROR ANALYSIS FOR RETRIEVED BATHYMETRY

Data Property	Proposed method	Channel			Basin				
		IDW	Kriging	Proposed method	IDW	Kriging	Proposed method	IDW	Kriging
Maximum	5.30	6.95	6.96	5.3	6.95	6.96	1.09	1.25	1.26
Mean	0.36	0.43	0.41	0.58	0.66	0.68	0.24	0.29	0.29
RMSE	0.69	0.73	0.72	0.82	0.92	0.93	0.39	0.42	0.42

(the long, deep, and narrow region and the broad, flat, elevated region within the study area, respectively) for further analysis (see Fig. 11(d); Table IX). It is clear that the errors in retrieved bathymetry of the channel area are relatively large, with maximum error greater than 5 m and mean error greater than 0.5 m. In fact, this agrees with the results presented above because water depth in this region is relatively high, often exceeding 15 m; such depths offer little useful information for remotely sensed images owing to water properties [5]. Moreover, the channel is

an area in which topography fluctuates and the retrieval of this complex topography requires denser sonar data. In spite of the low accuracy of the retrieved results, our proposed approach certainly offers the most compelling characteristics: maximum error of 5.3 m, mean error of 0.58 m, and RMSE of 0.82 m. Conversely, all three methods retrieve bathymetry with high accuracy in the basin area. The maximum and mean errors for our proposed approach are 1.09 and 0.24 m, respectively; these errors are extremely small. In general, the results of our

global error analysis indicate that the proposed approach always obtains higher accuracy bathymetry than that retrieved using IDW or kriging.

V. CONCLUSION

We have presented a workflow that integrates hyperspectral and sonar data for bathymetry mapping, allowing us to extract homogeneous regions from hyperspectral images and interpolate sonar points in each homogeneous region. We proposed a new algorithm, i.e., sonar-based semisupervised LE using spatial and spectral distance metrics, for the dimensional reduction of Hyperion images. During the interpolation of sparse sonar points, we also proposed a 3-D information diffusion method with homogeneous regions. Conclusions can be summarized as follows.

- 1) The proposed dimensional reduction method can achieve better dimensional results than unsupervised LE and semisupervised LE using only spectral distance metrics, which are related more closely to water depth and allow easier identification and classification.
- 2) The 3-D information diffusion interpolation method with homogeneous regions can retrieve bathymetry with much higher accuracy than common interpolation methods. The product of our proposed approach illustrates good stability in various strategies of comparisons, benefiting from the use of complementarity between sonar data and optical remote sensing imagery.

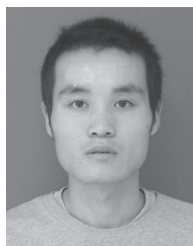
ACKNOWLEDGMENT

The authors would like to thank the anonymous reviewers and members of the editorial team for their comments and contributions.

REFERENCES

- [1] L. G. Leu and H. W. Chang, "Remotely sensing in detecting the water depths and bed load of shallow waters and their changes," *Ocean Eng.*, vol. 32, no. 10, pp. 1174–1198, Jul. 2005.
- [2] Ö. Ceyhan and A. Yalçın, "Remote sensing of water depths in shallow waters via artificial neural networks," *Estuarine Coastal Shelf Sci.*, vol. 89, no. 1, pp. 89–96, Sep. 2010.
- [3] A. Minghelli-Roman, A. Goreac, S. Mathieu, M. Spigai, and P. Gouton, "Comparison of bathymetric estimation using different satellite images in coastal sea waters," *Int. J. Remote Sens.*, vol. 30, no. 21, pp. 5737–5750, Oct. 2009.
- [4] Z. Lee *et al.*, "Water and bottom properties of a coastal environment derived from Hyperion data measured from the EO-1 spacecraft platform," *J. Appl. Remote Sens.*, vol. 1, no. 1, p. 11502, Dec. 2007.
- [5] J. Gao, "Bathymetric mapping by means of remote sensing: Methods, accuracy and limitations," *Prog. Phys. Geog.*, vol. 33, no. 1, pp. 103–116, May 2009.
- [6] S. R. Pillai, H. S. Oh, and A. Antoniou, "A new estimation technique for high-resolution bathymetry," *Signal Process.*, vol. 80, no. 5, pp. 809–818, May 2000.
- [7] S. Elvenes, M. F. Dolan, P. A. L. Buhl-Mortensen, and V. E. R. K. Bellec, "An evaluation of compiled single-beam bathymetry data as a basis for regional sediment and biotope mapping," *ICES J. Mar. Sci.*, vol. 71, no. 4, pp. 867–881, Oct. 2013.
- [8] R. Quinn and D. Boland, "The role of time-lapse bathymetric surveys in assessing morphological change at shipwreck sites," *J. Archaeolog. Sci.*, vol. 37, no. 11, pp. 2938–2946, Nov. 2010.
- [9] K. M. Marks and W. H. F. Smith, "An uncertainty model for deep ocean single beam and multibeam echo sounder data," *Mar. Geophys. Res.*, vol. 29, no. 4, pp. 239–250, Dec. 2008.
- [10] A. Kanno, Y. Koibuchi, and M. Isobe, "Statistical combination of spatial interpolation and multispectral remote sensing for shallow water bathymetry," *IEEE Geosci. Remote Sens. Lett.*, vol. 8, no. 1, pp. 64–67, Jan. 2011.
- [11] D. F. Watson, *Contouring: A Guide to the Analysis and Display of Spatial Data*. New York, NY, USA: Pergamon, 1992.
- [12] L. Mitas and H. Mitasova, "Spatial interpolation," in *Geographical Information Systems: Principles, Techniques, Management and Applications*, vol. 481. Hoboken, NJ, USA: Wiley, 1999.
- [13] J. Li and A. D. Heap, "A review of comparative studies of spatial interpolation methods in environmental sciences: Performance and impact factors," *Ecol. Inf.*, vol. 6, no. 3–4, pp. 228–241, Jul. 2011.
- [14] C. J. Calkoen, G. H. F. M. Hesselmanns, G. J. Wensink, and J. Vogelzang, "The Bathymetry assessment System: efficient depth mapping in shallow seas using radar images," *Int. J. Remote Sens.*, vol. 22, no. 15, pp. 2973–2998, Nov. 2010.
- [15] Z. Lee, K. L. Carder, C. D. Mobley, R. G. Steward, and J. S. Patch, "Hyperspectral remote sensing for shallow waters. 2. Deriving bottom depths and water properties by optimization," *Appl. Opt.*, vol. 38, no. 18, pp. 3831–3843, Jun. 1999.
- [16] L. Cheng *et al.*, "Integration of Lidar data and optical multi-view images for 3-D reconstruction of building roofs," *Opt. Lasers Eng.*, vol. 51, no. 4, pp. 493–502, Apr. 2013.
- [17] L. Tong, L. Cheng, M. Li, J. Wang, and P. Du, "Integration of LiDAR data and orthophoto for automatic extraction of parking lot structure," *IEEE J. Sel. Topics Appl. Earth Observ. Remote Sens.*, vol. 7, no. 2, pp. 503–514, Feb. 2014.
- [18] L. Cheng, J. Gong, M. Li, and Y. Liu, "3D building model reconstruction from multi-view aerial imagery and Lidar data," *Photogramm. Eng. Remote Sens.*, vol. 77, no. 2, pp. 125–139, 2011.
- [19] Z. Lee and K. L. Carder, "Effect of spectral band numbers on the retrieval of water column and bottom properties from ocean color data," *Appl. Opt.*, vol. 41, no. 12, pp. 2191–2201, Apr. 2002.
- [20] V. E. Brando and A. G. Dekker, "Satellite hyperspectral remote sensing for estimating estuarine and coastal water quality," *IEEE Trans. Geosci. Remote Sens.*, vol. 41, no. 6, pp. 1378–1387, Jun. 2003.
- [21] W. Ji, D. L. Civco, and W. C. Kennard, "Satellite remote bathymetry: A new mechanisms for modeling," *Photogramm. Eng. Remote Sens.*, vol. 58, no. 5, pp. 545–549, 1992.
- [22] W. D. Philpot, "Bathymetric mapping with passive multispectral imagery," *Appl. Opt.*, vol. 28, no. 8, pp. 1569–1578, 1989.
- [23] C. D. Mobley, *Hydrolight 4.0 Users Guide*. Bellevue, WA, USA: Sequoia Scientific, Nov. 1998.
- [24] D. R. Lyzenga, N. P. Malinas, and F. J. Tanis, "Multispectral bathymetry using a simple physically based algorithm," *IEEE Trans. Geosci. Remote Sens.*, vol. 44, no. 8, pp. 2251–2259, Aug. 2006.
- [25] C. J. Legleiter and D. A. Roberts, "A forward image model for passive optical remote sensing of river bathymetry," *Remote Sens. Environ.*, vol. 113, no. 5, pp. 1025–1045, May 2009.
- [26] F. C. Polcyn and D. R. Lyzenga, "Calculations of water depth from ERTS-MSS data," NASA Goddard Space Flight Center Marine Resour. Ocean Surv., Greenbelt, MD, USA, Mar. 1973, p. 159.
- [27] F. C. Polcyn and I. J. Sattinger, "Water depth determinations using remote sensing techniques," in *Proc. 6th Int. Symp. Remote Sens. Environ.*, Oct. 1969, vol. 2, pp. 13–16.
- [28] D. Spitzer and R. Dirks, "Bottom influence on the reflectance of the sea," *Int. J. Remote Sens.*, vol. 8, no. 3, pp. 279–308, Mar. 1987.
- [29] P. N. Bierwirth, T. J. Lee, and R. V. Burne, "Shallow sea-floor reflectance and water depth derived by unmixing multispectral imagery," *Photogramm. Eng. Remote Sens.*, vol. 59, no. 3, pp. 331–338, 1993.
- [30] D. R. Lyzenga, "Remote sensing of bottom reflectance and water attenuation parameters in shallow water using aircraft and Landsat data," *Int. J. Remote Sens.*, vol. 2, no. 1, pp. 71–82, Jan. 1981.
- [31] A. P. Cracknell and M. Ibrahim, "Bathymetry studies on the coastal waters (Red Sea) of Jeddah, Saudi Arabia, using shuttle MOMS-01 data," *Int. J. Remote Sens.*, vol. 9, no. 6, pp. 1161–1165, Jun. 1988.
- [32] J. C. Sandidge and R. J. Holyer, "Coastal bathymetry from hyperspectral observations of water radiance," *Remote Sens. Environ.*, vol. 65, no. 3, pp. 341–352, Sep. 1998.
- [33] H. S. Seung and D. D. Lee, "The manifold ways of perception," *Science*, vol. 290, no. 5500, pp. 2268–2269, Dec. 2000.
- [34] J. B. Tenenbaum, V. De Silva, and J. C. Langford, "A global geometric framework for nonlinear dimensionality reduction," *Science*, vol. 290, no. 5500, pp. 2319–2323, Dec. 2000.
- [35] S. T. Roweis and L. K. Saul, "Nonlinear dimensionality reduction by locally linear embedding," *Science*, vol. 290, no. 5500, pp. 2323–2326, Dec. 2000.

- [36] M. Belkin and P. Niyogi, "Laplacian eigenmaps and spectral techniques for embedding and clustering," in *Proc. Adv. Neural Inf. Process. Syst.*, 2001, vol. 14, pp. 585–591.
- [37] X. He, S. Yan, Y. Hu, and H. J. Zhang, "Learning a locality preserving subspace for visual recognition," in *Proc. IEEE Int. Conf. Comput. Vis.*, Nice, France, 2003, vol. 1, pp. 385–392.
- [38] Z. Zhang and H. Zha, "Principal manifolds and nonlinear dimensionality reduction via tangent space alignment," (English Edition), *J. Shanghai Univ.*, vol. 8, pp. 406–424, 2004.
- [39] C. M. Bachmann *et al.*, "Bathymetric retrieval from hyperspectral imagery using manifold coordinate representations," *IEEE Trans. Geosci. Remote Sens.*, vol. 47, no. 3, pp. 884–897, Mar. 2009.
- [40] D. Lungu, S. Prasad, M. Crawford, and O. Ersoy, "Manifold-learning-based feature extraction for classification of hyperspectral data: A review of advances in manifold learning," *IEEE Signal Process. Mag.*, vol. 31, no. 1, pp. 55–66, Jan. 2014.
- [41] X. Yang, H. Fu, H. Zha, and J. Barlow, "Semi-supervised nonlinear dimensionality reduction," in *Proc. 23rd Int. Conf. Mach. Learn.*, New York, NY, USA, 2006, pp. 1065–1072.
- [42] S. Ly, C. Charles, and A. Degre, "Geostatistical interpolation of daily rainfall at catchment scale: The use of several variogram models in the Ourthe and Ambleve catchments, Belgium," *Hydrol. Earth Syst. Sci.*, vol. 15, no. 7, pp. 2259–2274, Jul. 2011.
- [43] J. M. Schuurmans, M. F. P. Bierkens, E. J. Pebesma, and R. Uijlenhoet, "Automatic prediction of high-resolution daily rainfall fields for multiple extents: The potential of operational radar," *J. Hydrometeorol.*, vol. 8, no. 6, pp. 1204–1224, Dec. 2007.
- [44] C. A. Velasco-Forero, D. Sempere-Torres, E. F. Cassiraga, and J. J. Gómez-Hernández, "A non-parametric automatic blending methodology to estimate rainfall fields from rain gauge and radar data," *Adv. Water Resour.*, vol. 32, no. 7, pp. 986–1002, Jul. 2009.
- [45] R. Schiemann *et al.*, "Geostatistical radar-raingauge combination with nonparametric correlograms: Methodological considerations and application in Switzerland," *Hydrol. Earth Syst. Sci.*, vol. 15, no. 5, pp. 1515–1536, May 2011.
- [46] K. N. Dirks, J. E. Hay, C. D. Stow, and D. Harris, "High-resolution of rainfall on Norfolk Island, Part II: Interpolation of rainfall data," *J. Hydrol.*, vol. 208, no. 3/4, pp. 187–193, Jul. 1998.
- [47] M. C. Rogelis and M. Werner, "Spatial interpolation for real-time rainfall field estimation in areas with complex topography," *J. Hydrometeorol.*, vol. 14, no. 1, pp. 85–104, Feb. 2013.
- [48] D. G. Goodenough *et al.*, "Processing Hyperion and ALI for forest classification," *IEEE Trans. Geosci. Remote Sens.*, vol. 41, no. 6, pp. 1321–1331, Jun. 2003.
- [49] B. X. Tan, Z. Y. Li, E. X. Chen, and Y. Pang, "Preprocessing of hyperspectral image EO-1 Hyperion," *Remote Sens. Inf.*, no. 6, pp. 36–41, 2005.
- [50] L. F. Zhang, L. P. Zhang, D. C. Tao, and X. Huang, "On combining multiple features for hyperspectral remote sensing image classification," *IEEE Trans. Geosci. Remote Sens.*, vol. 50, no. 3, pp. 879–893, Mar. 2012.
- [51] L. P. Zhang, L. F. Zhang, D. C. Tao, and X. Huang, "Tensor discriminative locality alignment for hyperspectral image spectral-spatial feature extraction," *IEEE Trans. Geosci. Remote Sens.*, vol. 51, no. 1, pp. 242–256, Jan. 2013.
- [52] A. Mohan, G. Sapiro, and E. Bosch, "Spatially coherent nonlinear dimensionality reduction and segmentation of hyperspectral images," *IEEE Geosci. Remote Sens. Lett.*, vol. 4, no. 2, pp. 206–210, Apr. 2007.
- [53] D. J. Robinson, N. J. Redding, and D. J. Crisp, "Implementation of a fast algorithm for segmenting SAR imagery," *Electron. Res. Lab. Salisbury*, SA, Australia, Jan. 2002.
- [54] C. F. Huang, "Information diffusion techniques and small-sample problem," *Int. J. Inf. Technol. Decision Making*, vol. 1, no. 2, pp. 229–249, 2002.
- [55] P. Z. Wang, "A factor space approach to knowledge representation," *Fuzzy Sets Syst.*, vol. 36, no. 1, pp. 113–124, May 1990.



Lei Ma received the B.S. and M.S. degrees in cartography from Southwest Jiaotong University, Chengdu, China, in 2008 and 2011, respectively. He is currently working toward the Ph.D. degree in geography at the Jiangsu Provincial Key Laboratory of Geographic Information Science and Technology, Nanjing University, Nanjing, China.

His research interests include remote sensing image processing and geographic information systems.



Wenting Cai received the M.S. degree in cartography from Nanjing University, Nanjing, China, in 2012.

She is currently an Engineer with the Guangdong Electric Power Design Institute of China Energy Engineering Group, Guangdong, China. Her research interest is geographic information systems.



Lihua Tong received the Master's degree in geographic information sciences from Nanjing University, Nanjing, China, in 2014.

His research interests include remote sensing image processing and 3-D reconstruction.



Manchun Li received the Ph.D. degree in cartography from Nanjing University, Nanjing, China, in 1992.

He is currently a Professor with the Jiangsu Provincial Key Laboratory of Geographic Information Science and Technology, Nanjing University. His research interests include geographic information systems and remote sensing applications.



Peijun Du received the Ph.D. degree in photogrammetry and remote sensing from the China University of Mining and Technology, Jiangsu, China, in 2001.

He is currently a Professor of photogrammetry and remote sensing with the Department of Geographic Information Sciences, Nanjing University, Nanjing, China. His research interests include multisource geospatial information fusion and spatial data handling, integration and applications of geospatial information technologies, and environmental information science.

Dr. Du serves as the Associate Editor of the IEEE GEOSCIENCE AND REMOTE SENSING LETTERS.



Liang Cheng received the Ph.D. degree in photogrammetry and remote sensing from Wuhan University, Wuhan, China, in 2008.

He is currently an Associate Professor with the Jiangsu Provincial Key Laboratory of Geographic Information Science and Technology, Nanjing University, Nanjing, China. He has published over 40 papers in international journals. His research interests include integration of multisource spatial data and remote sensing image processing.